Structural, morphological and optical characterization of ZnO/TiO_2 multi-layer nanocomposites extracted from commercial sunscreens

L. G. DAZA[1], E. A. MARTÍN-TOVAR[2,*], M. DUARTE-AKÉ[1], I. V. PEREZ-QUINTANA[1], R. CASTRO-RODRIGUEZ[3]
[1]*Faculty of Engineering, Autonomous University of Yucatan, Merida A.P. 150/97203, Mexico*
[2] *División de Oncología y Uronefrología, Departamento de Radioterapia, Unidad Médica de Alta Especialidad, Hospital de Especialidades del Centro Médico Nacional "Ignacio García Téllez", Instituto Mexicano del Seguro Social, CP 97150 Mérida, Yucatán, México*
[3]*Applied Physics Department, CINVESTAV-IPN, Merida A.P. 73/97205, Mexico*

ZnO, TiO_2, and ZnO/TiO_2 multilayer nanocomposites extracted from commercial sunscreens and protective gel were prepared using the Sol-Gel Spin-Coating (SGSC) technique. SEM analysis revealed three-dimensional spherical structures with maximum thicknesses of 4.67, 3.08, and 1.52 mm for ZnO, TiO_2, and ZnO/TiO_2 layers, respectively. XRD confirmed polycrystalline, mesoporous films with hexagonal wurtzite (ZnO) and tetragonal anatase (TiO_2) phases. Analysis by X-ray spectroscopy (EDS) detected ZnO and TiO_2 without elemental impurities. Optical transmittance ranged from 10% to 40% in the 300-850 nm wavelength region. These properties suggest potential suitability for dye-sensitized solar cells.

(Received December 24, 2024; accepted August 5, 2025)

Keywords: Sunscreen, ZnO, TiO_2, Sol-gel, Spin-coating, Nanocomposites

1. Introduction

The unique properties and broad application range of metal oxides have made them extensively studied nanomaterials. Zinc oxide (ZnO) and titanium dioxide (TiO_2) are two prominent examples. Both nanomaterials are essential in applications such as photocatalysts, optoelectronics, sensors, and electronic devices [1-3]. In particular, their remarkable ability to scatter and absorb ultraviolet (UV) radiation has made them essential components in the formulation of commercial sunscreens, as they provide superior sun protection and aesthetic improvements [4, 5].

Despite their widespread use, significant gaps remain in the understanding the properties of ZnO and TiO_2-based nanomaterials in commercial products. Product labels often fail to provide detailed information about the nanoparticles' morphology, dimensions, crystalline phase, or composition [6, 7]. This lack of characterization hinders the systematic evaluation of safety, environmental impact and performance under real-world conditions.

In this study, we propose and validate a robust methodology to obtain ZnO and TiO_2 nanoparticles for thin film preparation using the sol-gel spin-coating (SGSC) technique with materials extracted directly from commercial sunscreens. This approach differs from conventional methods that rely on synthesizing new materials. Recent advancements in the synthesis of ZnO and TiO_2 nanostructures have predominantly focused on physical, chemical, and hydrothermal methods, which often involve high energy consumption, costly precursors, and environmentally challenging procedures [8-11]. While these approaches enable precise control over nanostructure morphology and properties, their scalability and ecological footprint pose significant limitations for large-scale or sustainable applications. In contrast, the extraction of nanostructured materials from consumer-end products, such as commercial sunscreens, represents a pioneering strategy aligned with principles of green chemistry and waste valorization. Such approaches leverage readily available, low-cost, and already functionalized materials, circumventing the need for elaborate synthesis procedures [12]. Our work introduces a novel, environmentally friendly alternative by extracting ZnO/TiO_2 nanocomposites directly from commercially available sunscreens—a resource rich in nanosized ZnO and TiO_2 particles designed to maximize UV absorption and photostability, reducing environmental impact and manufacturing costs.

Results revealed the formation of 3D spherical structures, confirming the mesoporous and polycrystalline nature of the synthesized materials. The hexagonal wurtzite (ZnO) and tetragonal anatase (TiO_2) phases were identified. Moreover, UV-Vis optical transmittance evaluation underscores their effectiveness as photoprotective materials. This work not only advances the understanding of ZnO/TiO_2 nanocomposites in consumer products but also provides a valuable comparative framework against laboratory-synthesized nanoparticles. These findings highlight the need for application-oriented material characterization and its real-world implications.

2. Materials and methods

ZnO samples were obtained by diluting a commercial gel called Dr. Bell´s skin ointment (Genomma lab USA Inc) in mineral oil at a ratio of ∼1:5, i.e., 5 ml of mineral oil was added for each gram of commercial gel, resulting in a suitable viscosity for application to a glass substrate. To prevent the formation of agglomerates, the solution was subjected to an ultrasonic bath for 20 minutes. Subsequently, four drops (∼0.05 ml per drop) of the solution were applied to a commercial glass substrate previously cleaned by sequential ultrasonic baths in acetone, ethanol, isopropyl alcohol and deionized water for 5 minutes each. Subsequently, by the sol-gel spin coating method, different rotation speeds were applied: initially, at 220 rpm for 15 seconds, then at 560 rpm for another 15 seconds and finally at 810 rpm for another 15 seconds. The result was a thin layer of the material, which was heat treated by heating it from 450°C to 550°C for 20 minutes to eliminate the organic components present in the mineral oil and commercial gel. This method provided a functional ZnO film on the substrate. To deposit ZnO with a different number of layers, the process was repeated 6 (ZnO_06), 8 (ZnO_08) and 12 (ZnO_12) times. To obtain the TiO_2 samples, a commercial SimiBlock sunscreen (Farmacias de Similares S.A. de C.V.) was diluted in distilled water using a ratio of ∼1:8, i.e., 8 ml of distilled water were added for every gram of commercial sunscreen, achieving a consistency suitable for the SGSC. A process equivalent to that for obtaining the ZnO samples was subsequently performed, using an ultrasonic bath for 20 min, depositing 4 drops of the resulting mixture (∼0.05 ml per drop) on a previously cleaned glass substrate using SGSC at 220 rpm for 15 seconds, then at 560 rpm for another 15 seconds, and finally at 810 rpm for another 15 seconds. The process was repeated 6 (TiO_2_06), 8 (TiO_2_08) and 12 (TiO_2_12) times. To obtain the ZnO/TiO_2 nanocomposite multilayers, each material was deposited alternately one after another using the same SGSC procedure described above. Three samples marked as Mx_06, Mx_08 and Mx_12 were created corresponding to samples with 6, 8, and 12 layers of the combined TiO_2 and ZnO nanocomposite multilayers, respectively.

Structural analysis was accomplished using X-ray diffraction (XRD) in the grazing incidence geometry with an inclination of 1° using a D5000 Siemens X-ray diffractometer and Cu Kα radiation (λ=1.5406 Å). The diffractograms were registered in the step scan mode with a beam incidence angle of 1° and recorded in 0.02° steps with a step time of 10 s in a 2θ range of 20°−80°. Surface and cross-sectional images of the nanocomposite films were obtained by a JEOL 7600F field emission scanning electron microscope (FESEM). The percentage of constituent elements was evaluated by energy dispersive spectroscopy (EDS). The transmittance spectra were recorded with an Agilent 8453 UV-Vis spectrophotometer with a 0.1 nm resolution, in the range of 300−1100 nm.

3. Results and discussion

3.1. SEM analysis

For morphological analysis, the samples were examined by scanning electron microscopy (SEM). Fig. 1 shows the surface and profile SEM images for the 12-layer nanocomposite multilayers, for the three different type samples, namely, ZnO, TiO_2 and ZnO/TiO_2. For the ZnO_12 sample, Fig. 1 (a) and (b) show surface and profile images with an amplification of x10000 and x5000, respectively. Similar images were obtained for the other ZnO samples; therefore, we considered ZnO_12 representative of the others. A homogeneous and uniform layer with a mesoporous arrangement of ZnO nano- and microstructures with variable geometries (cubes, spheres, planes and rods with hexagonal shapes) stacked on top of each other is observed. For the TiO_2_12 sample, Fig. 1 (c) and (d) show surface and profile images with an amplification of x10000 and x5000, respectively. Similar images were obtained for the other TiO_2 samples; therefore, we considered TiO_2_12 representative of the others. In these samples, a homogeneous and uniform layer with a mesoporous arrangement of spherical clusters of TiO_2 nanostructures stacked on top of each other is also observed. For the Mx_12 sample, Fig. 1 (e) and (f) show surface and profile images with an amplification of x10000 and x5000, respectively. Similar images were obtained for the combined TiO_2 and ZnO nanocomposite multilayers, therefore we considered Mx_12 as representative of the others. In these samples, ZnO and TiO_2 nanostructures next to each other with geometries like those obtained for the pure ZnO and TiO_2 samples were observed. It is also shown that the TiO_2 nanostructures, being smaller than those of ZnO, are "attached" to the larger ZnO structures. The presence of three-dimensional structures in all three groups of samples allows us to infer that the layers have a greater proportion of surface area and therefore a greater capture of electrical charges. All the nanostructures on the three groups of samples are stacked on top of each other and therefore can be seen as a mesoporous system. Using the free software ImageJ [13], a treatment was performed on the SEM surface images (not shown in the figures), where porosity values between 30% and 40% were obtained for all the grown samples. The average thickness of the multilayer nanocomposites was determined from profile SEM images; the obtained values are shown in Table 1.

Table 1. Thickness measurements of deposited layers: ZnO, TiO_2, and ZnO/TiO_2 composites as a function of deposition cycles (6, 8, and 12 layers)

	6 layers (μm)	**8 layers** (μm)	**12 layers** (μm)
ZnO	1.425	1.856	4.669
TiO_2	0.459	0.778	3.075
ZnO/TiO_2	1.331	1.069	1.519

The thickness in ZnO samples increased from 1.4 μm to 4.6 as the number of layers increased. Similarly, for the TiO_2 samples, the thickness values ranged from 0.4 to 3.1 μm, increasing as a function of the number of layers. For the combined nanocomposite multilayer samples of ZnO and TiO_2, the values obtained for all layers have an average value close to 1.4 μm. In the inset of the SEM surface images for the three groups of samples (Fig. 1 (a), (b), and (c)), it can be seen that agglomerates of nanoparticles were obtained with shapes ranging from spheres to cylinders, with approximate sizes between 142 to 474 nm for the ZnO deposits, 150 to 241 nm for the TiO_2 deposits, and 172 to 452 nm for the combined Mx deposits.

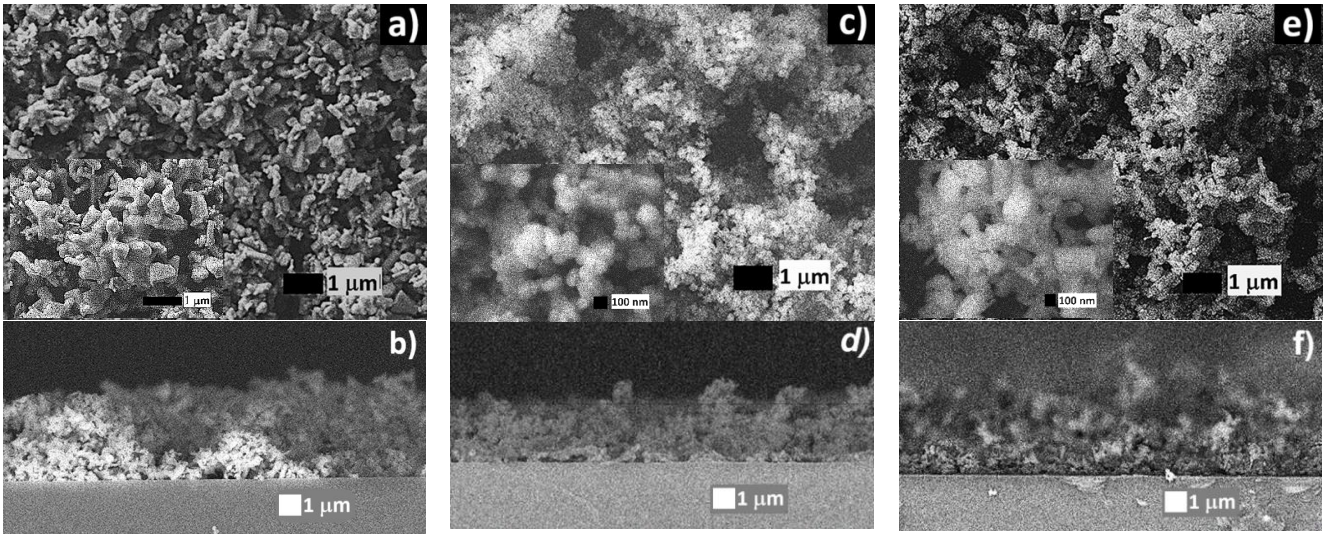

Fig. 1. SEM images of 12-layer samples: a) Surface and b) cross-section of ZnO; c) Surface and d) cross-section of TiO_2; e) Surface and f) cross-section of ZnO/TiO_2 composite. Insets: Higher magnification views of corresponding surface morphologies

The EDS analysis for the ZnO multilayer nanocomposite is given in Fig. 2 (a). The typical peaks of oxygen and zinc are identified. The presence of other elements was not found, suggesting that the heating process eliminated the organic elements present in the commercial gel. The weight and atomic percentages of Zn and O were 76.76; 23.24 and 44.71; 55.29, respectively. This agrees with what is reported in the literature for the weight percentage of ZnO (80% for Zn and 20% for O) [14]. The small peaks shown in Fig. 2 (a) could not be identified by the EDS analysis. These peaks can be attributed to negligible traces of other elements or to noise in the measurement signal. The EDS spectrum for TiO_2 nanocomposite multilayers is shown in Fig. 2 (b). The presence of peaks corresponding to Ti and O is clearly observed, while no peaks from other elements were detected. This further indicates that the heating process effectively removed organic components present in the commercial gel. The weight and atomic percentages of Ti and O were 43.79.; 56.21 and 20.65; 79.35, respectively. This agrees with what is reported in the literature for the weight percentage of TiO_2 (80% for O and 20% for Ti) [15]. The EDS analysis of the ZnO/TiO_2 nanocomposite multilayers was performed, and the results are shown in Fig. 2 (c). The presence of Ti, Zn and O was proven by EDS analysis. No peaks corresponding to any other element are found. This indicates that the remaining organic components from both commercial sunscreens were effectively removed by the heating process. The weights and atomic concentrations for Zn: Ti:O ratio was 49.58:4.37:45.04 and 20.35:2.45:77.20, respectively. The quantitative estimations of weight and atomic percentage for all three figures is presented in the inset figure.

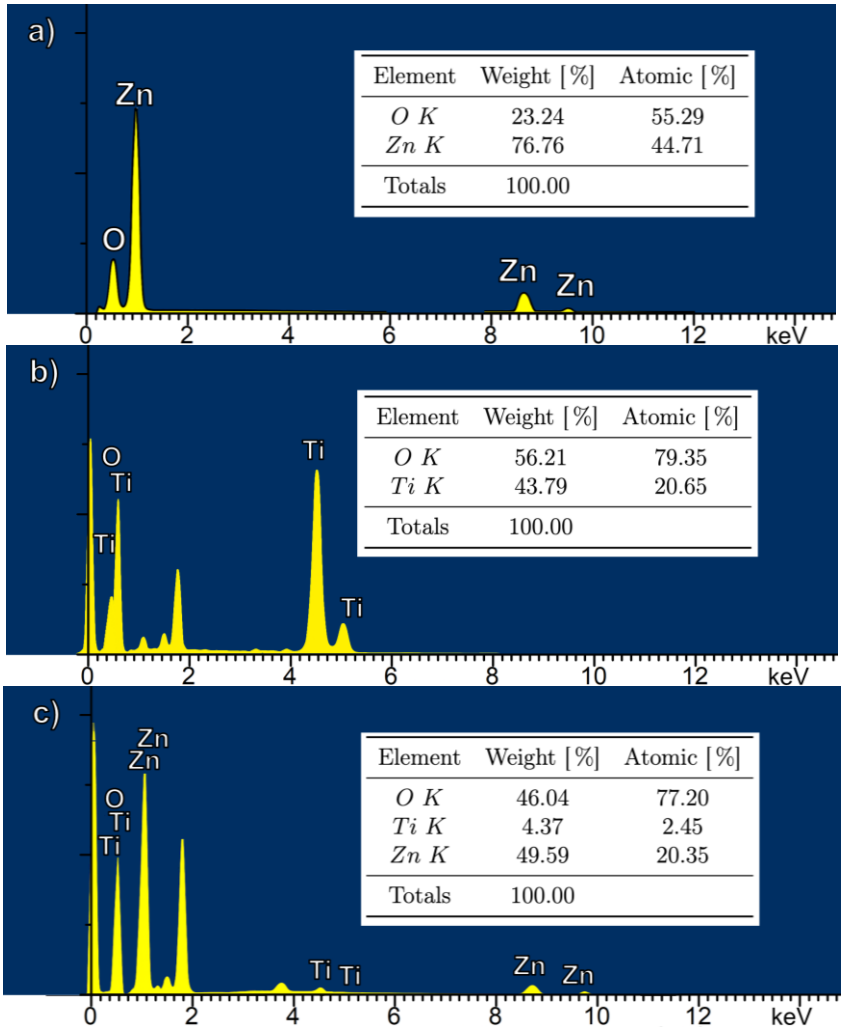

Fig. 2. EDS spectra of: ZnO; TiO_2; c) ZnO/TiO_2. Insets: Quantitative elemental composition (weight% and atomic%). All data from 12-layer samples (colour online)

3.2. X-ray diffraction analysis

Using the X-ray diffraction technique, the diffraction spectra were obtained for the ZnO, TiO_2 and ZnO/TiO_2 samples as shown in Fig. 3. The spectra in Fig. 3 (a) and (b) corresponded to JCPDS 36-1451 letter [16]. The XRD pattern of the ZnO samples shows the characteristic peaks of the hexagonal Wurtzite structure [17], with the most intense reflection observed at the (101) plane. Additional reflections are observed in the (100), (002), (102), (110), (103) and (112) planes, indicating the polycrystalline nature of these samples. This is likely because the commercial gel from which the ZnO was extracted is essentially just ZnO powder embedded within an organic matrix. The ZnO powder synthesized through a predefined chemical process established by the manufacturer, resulting in materials with specific structural, morphological, and optical characteristics. A comparison between the standard diffraction angles and those observed in our samples reveals a slight shift to the right, suggesting a compressive stress in the ZnO crystal lattice [18, 19]. This shift may be attributed to structural defects, such as oxygen vacancies, within the crystal lattice. To determine the crystallite size of all samples, we considered Scherrer's formula, which is given by [10]:

$$D = \frac{k\lambda}{\beta\cos\theta} \tag{1}$$

where D is the mean crystallite size, k = 0.9 the shape factor, θ is the diffraction angle, β is the full width at half maxima (FWHM) and λ is the X-ray wavelength (0.15418 nm). As shown in Table 2, crystallite ranging from 49 nm to 52 nm were calculated for the various ZnO layers. The lattice parameters were determined using the standard lattice geometry equation for a hexagonal structure [20]:

$$\frac{1}{d_{hkl}^2} = \frac{4}{3}\left(\frac{h^2+hk+k^2}{a^2}\right) + \frac{l^2}{c^2} \tag{2}$$

where a and c are the lattice constants, and d_{hkl} is the crystalline interplanar distance. The strain induced due to crystal imperfection and distortion was calculated using the formula [20]:

$$\varepsilon = \frac{\beta_{hkl}}{4tan\theta} \quad (3)$$

The values of crystallite size, strain, and lattice parameters for the ZnO samples with 6, 8 and 12 layers are shown in Table 2. For the TiO_2 samples, as shown in Fig. 3 (c) and (d), using the JCPDS chart 00-021-1272 [21], we observed that the structure is tetragonal anatase with the most intense reflection at the (101) plane. Additional prominent reflection peaks are observed at the (004), and (200) planes. Weaker intensity peaks corresponding to the (105), (211), (204), (220), (215) and (224) planes are also visible, indicating the polycrystalline nature of the samples. This is possibly due to a similar reason as with the ZnO samples, since the TiO_2 was also obtained from a commercial gel. Fig. 3 (b) shows the diffraction angles of the main peak (101) in each sample, they are compared with the position of the standard diffraction angle of TiO_2 and it is observed that they are slightly shifted to the right, this indicates a contraction stress of the TiO_2 crystal lattice, probably induced by structural defects due to oxygen vacancies. The average crystallite size was determined using the equation (1). The calculated crystallite sizes can be seen in Table 2 and their values range between 43 nm and 47 nm for the different TiO_2 layers. The lattice parameters for a tetragonal structure were calculated by [22]:

$$\frac{1}{d^2} = \frac{h^2+k^2}{a^2} + \frac{l^2}{c^2} \quad (4)$$

The values of crystallite size, strain and lattice parameters of the 6, 8 and 12 layers TiO_2 samples are shown in Table 2. Finally, as shown in Fig. 3 (e) and (f), the diffraction spectra were obtained for the ZnO/TiO_2 nanocomposite samples where the existence of ZnO hexagonal and TiO_2 anatase phase are evident. The films show sharp diffraction peaks indicating the high crystallinity of both ZnO and TiO_2. For ZnO, its plane of greatest reflection is (101), which is the largest in the entire sample, and (100), (002), (102), (110), (103) and (112). The plane of greatest reflection of TiO_2 is the (101) and a peak is also observed in the (200) plane. The spectra obtained in samples are very similar to each other and are also similar to those obtained by other authors of growth with significantly enhanced photocatalytic activity [23-26].

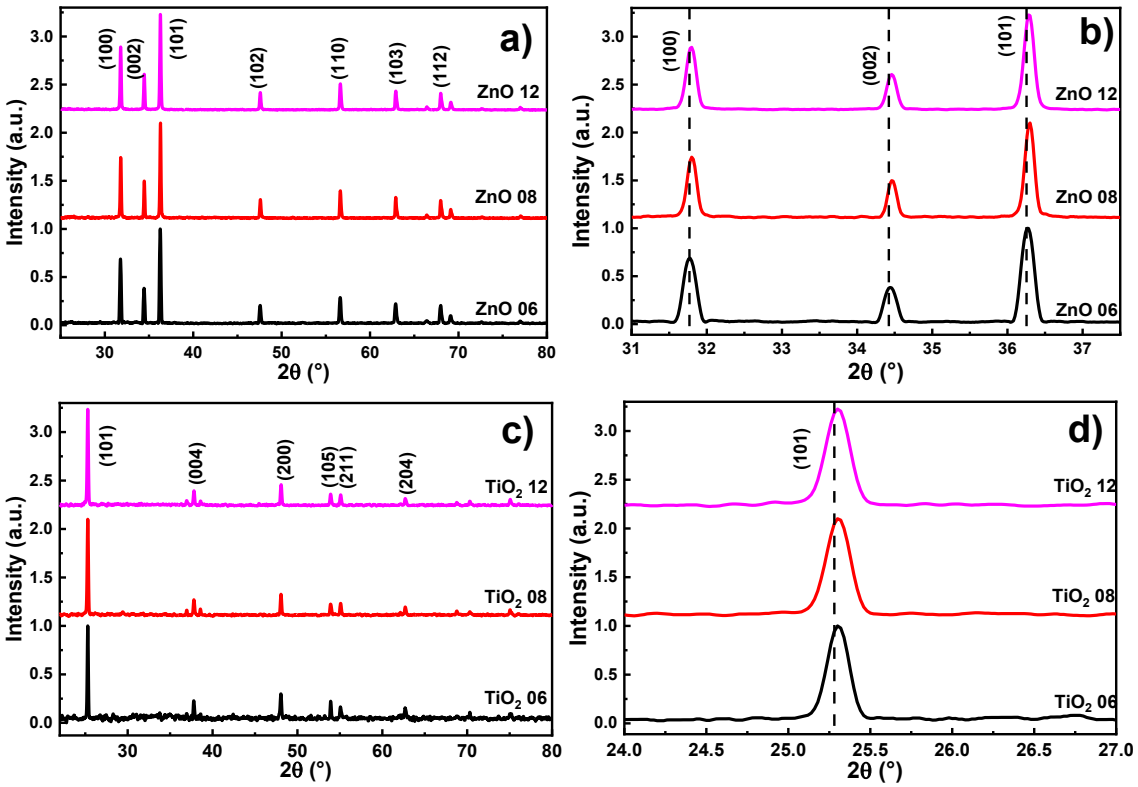

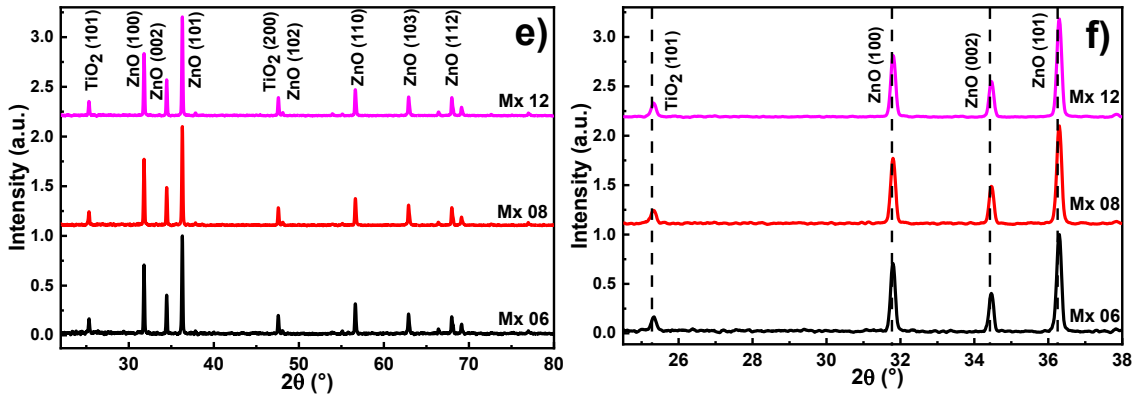

Fig. 3. XRD patterns: (a) ZnO, (b) ZnO peaks, (c) TiO_2, (d) TiO_2 peaks, (e) ZnO/TiO_2, (f) composite peaks (dashed lines: JCPDS) (colour online)

Table 2. Structural parameters of ZnO and TiO_2 samples: crystallite size (D), interplanar spacing (d), lattice constants (a, c), unit cell volume (V), and strain (ε)

Sample	D (nm)	d (Å)	$2\theta_{002}$ (°)	a (Å)	c (Å)	V $(Å)^3$	e $x10^{-3}$
Standard ZnO	-		34.422	3.249	5.206	47.592	-
ZnO 6c	50.83	2.038	34.458	3.247	5.201	47.491	1.777
ZnO 8c	52.94	2.038	34.466	3.246	5.200	47.467	1.709
ZnO 12C	49.06	2.038	34.460	3.247	5.201	47.502	1.842
Standard TiO_2	-		25.280	3.785	9.513	136.313	-
TiO_2 6c	47.49	1.844	25.303	3.784	9.529	136.457	1.786
TiO_2 8c	43.92	1.844	25.303	3.782	9.547	136.632	1.876
TiO_2 12C	45.35	1.820	25.301	3.781	9.569	136.879	1.820

3.3. Optical properties

The transmittance spectra of the multilayer ZnO nanocomposites deposited with SGSC is shown in Fig. 4 (a). There is an absorption edge (around 300 nm). In the wavelength region between 450 and 1100 nm, low transmittance was obtained. A possible explanation for the above is that the number of layers of material applied produces opaque samples. Fig. 4 (b) displays the optical transmittance of TiO_2 nanocomposite multilayers deposited by SGSC. In the wavelength range from 350 to 1100 nm, low transmittances values are also observed, approximately 40%, 20%, and 5% for the TiO_2_06, TiO_2_08 and TiO_2_12 samples, respectively. Fig. 4 (c) show the transmittance of the ZnO/TiO_2 nanocomposite multilayers. In the visible wavelength range (350 to 800 nm) low transmittances occur (less than 20% for the Mx_06 sample and below 10% for the rest of the samples). For wavelengths greater than 800 nm, a slight increase in transmittance is observed in all samples, but without exceeding 25% in any of them. The disordered stacking of the ZnO, TiO_2 and mixed ZnO/TiO_2 nanocomposite structures could favor light scattering, causing it to be trapped within the matrix of the disordered structure of the nanocomposite multilayers, reflecting the light inside the mesoporous matrix, and thus, preventing a transmittance beyond 20% within the visible region of light for all samples types. The results suggest that the nanocomposites developed in this study possess promising characteristics for potential application as photoelectrodes in dye-sensitized solar cells.

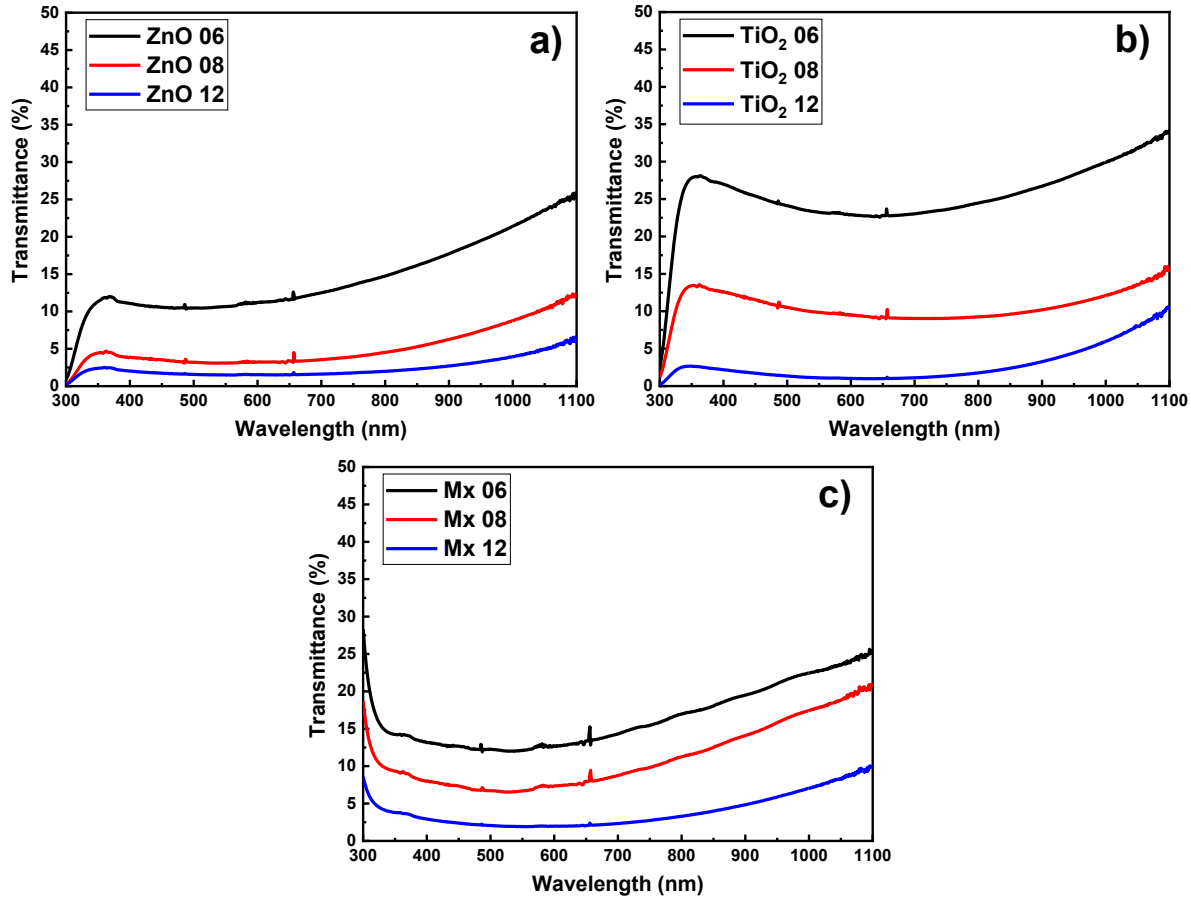

Fig. 4. Optical transmittance spectra (300-1100 nm) for: a) ZnO, b) TiO_2, and c) ZnO/TiO_2 nanocomposite multilayers, showing wavelength-dependent transmission characteristics (colour online)

4. Conclusions

In this work, multilayer nanocomposites composed of 6, 8 and 12 layers of ZnO, TiO_2 and a combination of both ZnO and TiO_2, extracted from commercial sunscreens were fabricated using the SGSC technique. Cross-sectional SEM images confirmed the formation of homogeneous multilayers structures, with thicknesses ranging from 1.4 µm to 4.6 µm for the ZnO samples, 0.5 µm to 3.1 µm for the TiO_2 samples, and 1.3 µm to 1.5 µm for the ZnO/TiO_2 composite samples, respectively. XRD analysis confirmed the high crystallinity of all three sample types. The crystallite sizes ranged between 49-53 nm for ZnO and 44-48 nm for the TiO_2. These dimensions are consistent with those typically associated with enhanced photocatalytic activity in the literature. The resulting nanocomposites exhibit promising structural and optical properties for potential applications as photoelectrodes in dye-sensitized solar cells (DSSCs).

Acknowledgments

The authors wish to thank Dr. Patricia Quintana for the help of their experimental characterization laboratories of National Council for Science and Technology of Mexico & Mixed Fund, Yucatan State Government with contract 2008-108160 and National Council for Science and Technology of Mexico under project numbers [2009-01-123913, 29-(2692, 4643), 188345, 204822]. The author L.G. Daza expresses gratitude to SECIHTI for the postdoctoral stay in 2022 (2) under the announcement "Postdoctoral Stays in Mexico for the Training and Consolidation of Researchers in Mexico." We also extend our thanks to Mario Herrera, Oswaldo Gómez and Daniel Aguilar, for their technical support and Alex Mora for secretarial assistance.

References

[1] S. Sakthivel, B. Neppolian, M. V Shankar, B. Arabindoo, M. Palanichamy, V. Murugesan, Sol. Energ. Mat. Sol. C. **77**, 65 (2003).
[2] C. W. Zou, J. Wang, and W. Xie, J. Colloid Interf. Sci. **478**, 22 (2016).
[3] R. A. Rahman, M. A. Zulkefle, K.A. Yusof, W. F. Abdullah, M. R. Mahmood, S. H. Herman, J. Teknol. **78**, 33 (2016).
[4] C. C. Lee, Y. H. Lin, W. C. Hou, M. H. Li, J. W. Chang, Int. J. Environ. Res. Public Health **17**(17), 6088 (2020).

[5] J. Pasquet, Y. Chevalier, E. Couval, D. Bouvier, M. A. Bolzinger, Int. J. Pharm. **479**, 88 (2015).
[6] C. Contado, Front. Chem. **3**, 48 (2015).
[7] W. J. Stark, P. R. Stoessel, W. Wohlleben, A. Hafner, Chem. Soc. Rev. **44** (16), 5793 (2015).
[8] R. Ghamarpoor, A. Fallah, M. Jamshidi, ACS Omega **9**, 25457 (2024).
[9] X. Liu, G. Wang, H. Zhi, J. Dong, J. Hao, X. Zhang, J. Wang, D. Li, B. Liu, Coatings **12**, 695 (2022).
[10] M. H. Fawey, A. A. Abd El-Moula, T. Hashem, M. Abo El-Kaseem, J. Mater. Sci.: Mater. Electron. **36**, 764 (2025).
[11] M. Sibinski, P. Sawicka-Chudy, G. Wisz, P. Gnida, E. Schab-Balcerzak, A. Wal, R. Yavorskyi, M. Cholewa, Sci. Rep. **14**, 10676 (2024).
[12] A. Gonçalves, P. Toledo, N. Joshi, M. Berengue, Molecules **26**, 2236 (2021).
[13] Z. Garduño, L.G. Daza, A. Iribarren, R. Castro-Rodríguez, Appl. Surf. Sci. **698**, 163080 (2025).
[14] M. S. Geetha, H. Nagabhushana, H. N. Shivananjaiah, J. Sci.: Adv. Mater. Devices. **1**, 301 (2016).
[15] M. Ramazani, M. Farahmandjou, T. P. Firoozabadi, Int. j. nanosci. nanotechnol. **11**, 115 (2015).
[16] R. Zhang, J. Xie, C. Wang, J. Liu, X. Zheng, Y. Li, X. Yang, H. Wang, B. Su, J. Mater. Sci. **52**, 11124 (2017).
[17] Z. A. Lewicka, A. F. Benedetto, D. N. Benoit, W. W. Yu, J. D. Fortner, V. L. Colvin, J. Nanoparticle Res. **13**, 3607 (2011).
[18] M. Sathya, K. Pushpanathan, Appl. Surf. Sci. **449**, 346 (2018).
[19] J. Panigua-Méndez, S. L. Ramírez-Sandoval, E. Reyes-Uribe, M. E. Contreras-García, Ceram. Int. **50**, 34421 (2024).
[20] M. Nabil, I. V. Perez-Quintana, M. Acosta, J. A. Mendez-Gamboa, R. Castro-Rodriguez, Adv. Mater. Sci. Eng. **2021**, 9926544 (2021).
[21] M. Xiao, K. P. Musselman, W. W. Duley, Y. N. Zhou, ACS. Appl. Mater. Interfaces. **9**, 4808 2017).
[22] X. Liu, J. Fu, Optik. **206**, 16342 (2020).
[23] D. Upadhaya, P. Kumar, D. D. Purkayastha, J. Mater. Sci. -Mater. El. **30**(11), 10399 (2019).
[24] Y. Yadawa, S. Singh, A. Ranjan, Materials Science and Engineering B **288**, 116164 (2023).
[25] A. Sharifi Rad, A. Afshar, M. Azadeh, Opt. Mater. **136**, 113501 (2023).
[26] K. Kusdianlo, D.F. Nugraha, A. Sekarnusa, S. Madhania M. Machmudah, S. Winardi, IOP Conf. Ser.: Mater. Sci. Eng. **1053**, 012024 (2021).

*Corresponding author: enrique.martin.tovar@gmail.com